

# Mechanical Design of the First Proximal Ig Domain of Human Cardiac Titin Revealed by Single Molecule Force Spectroscopy

Hongbin Li and Julio M. Fernandez\*

Department of Biological Sciences, Columbia University  
New York, NY 10027, USA

The elastic I-band part of muscle protein titin contains two tandem immunoglobulin (Ig) domain regions of distinct mechanical properties. Until recently, the only known structure was that of the I27 module of the distal region, whose mechanical properties have been reported in detail. Recently, the structure of the first proximal domain, I1, has been resolved at 2.1 Å. In addition to the characteristic  $\beta$ -sandwich structure of all titin Ig domains, the crystal structure of I1 showed an internal disulfide bridge that was proposed to modulate its mechanical extensibility *in vivo*. Here, we use single molecule force spectroscopy and protein engineering to examine the mechanical architecture of this domain. In contrast to the predictions made from the X-ray crystal structure, we find that the formation of a disulfide bridge in I1 is a relatively rare event in solution, even under oxidative conditions. Furthermore, our studies of the mechanical stability of I1 modules engineered with point mutations reveal significant differences between the mechanical unfolding of the I1 and I27 modules. Our study illustrates the varying mechanical architectures of the titin Ig modules.

© 2003 Elsevier Ltd. All rights reserved.

\*Corresponding author

**Keywords:** I1 Ig domain; titin; mechanical unfolding; AFM; single molecule

## Introduction

Titin, the third filament of muscle, is a giant muscle protein spanning half of the sarcomere from the Z disk to the M line with a contour length of more than 1  $\mu\text{m}$ .<sup>1,2</sup> Titin is responsible for the passive elasticity of muscle,<sup>3</sup> which plays an important role in muscle function.<sup>4</sup> The I-band of titin has been recognized to be elastic and responsible for the passive elasticity of muscle, while the A-band part of titin is inextensible and responsible for the organization of the sarcomeres.<sup>5–7</sup> Single myofibril studies and single molecule measurements, using atomic force microscopy (AFM) and optical tweezers, have demonstrated that titin is elastic and can extend under a mechanical stretching force.<sup>8–14</sup>

Titin has a modular structure and different types of muscles have differentially spliced titin isoforms. Titin contains ~300 immunoglobulin-

like (Ig) domains and fibronectin type III domains that are linked in series. In addition, titin also contains some unique sequences whose structures are not well defined and have features resembling that of random coil sequences.<sup>3,15</sup> The folded domains show low sequence homology amongst themselves (20–30% identity, 30–40% similarity between Ig modules in human skeletal titin<sup>16</sup>) and widely different thermodynamic stability<sup>17</sup> (2.55–7.36 kcal/mol). However, the key residues of individual Ig repeats across different species and the super-repeat patterns of avian and mammalian titins are highly conserved through evolution<sup>16</sup> (82.5% similarity between the human and the reptile sequences), suggesting that titin's modular structure is critical for the elasticity of titin. Hence, it is of great importance to determine the mechanical architecture of I-band titin and to understand how the elasticity is controlled by modulating titin's mechanical architecture through alternatively spliced isoforms in different muscles.

The I-band of human cardiac titin N2B isoform, the shortest isoform of titin, consists of four structurally distinct regions: proximal Ig and distal Ig regions, N2B unique sequence and the so-called

Abbreviations used: Ig, immunoglobulin; AFM, atomic force microscopy; SMD, steered molecular dynamics.

E-mail address of the corresponding author:  
jfernandez@columbia.edu

PEVK segment, 70% of its sequence are proline, glutamate, valine and lysine.<sup>3</sup> These four regions extend differentially under a mechanical stretching force in intact muscle, suggesting these four regions have different mechanical properties.<sup>14,18</sup> Single molecule AFM studies have demonstrated that the N2B and PEVK segments are flexible random-coil like sequences with different persistence length, a measure of molecule's flexibility.<sup>11,19,20</sup> Proximal and distal Ig domains on the contrary, share the same persistence length yet have very different extensibility. Combined studies on the distal Ig domain I27 (following the convention of Labeit & Kolmerer<sup>14</sup>) using single molecule AFM, protein engineering and molecular dynamics simulations have provided detailed insights into the mechanical unfolding of distal Ig domains.<sup>11,12,21-25</sup> I27 has a characteristic  $\beta$ -sandwich structure.<sup>26</sup> It has been shown that the regions, where the A-B and A'-G  $\beta$  strands overlap, allows I27 to resist mechanical unfolding. These two regions are termed as A-B and A'-G patches, respectively. A set of key backbone hydrogen bonds linking the A and B, A' and G  $\beta$  strands, are critical for the mechanical stability of I27.<sup>23,25,27</sup> We now know that distal Ig domains unfold through similar unfolding pathways that involve an unfolding intermediate state. This unfolding intermediate state provides extra mechanical resistance to distal Ig domains.<sup>11,12</sup> I27 has become the paradigm for single molecule AFM and modeling studies.<sup>12,21,23,25,27-32</sup> By contrast, our understanding of proximal Ig domains has been limited by the lack of detailed structural information.

Recently, the X-ray crystal structure of the first proximal Ig domain I1 has become available.<sup>33</sup> I1 is 100 amino acids long and has a characteristic  $\beta$ -sandwich structure with seven antiparallel  $\beta$  strands<sup>33</sup> (Figure 1), which is very similar to that of I27. The backbone hydrogen bonds linking the A-B and A'-G  $\beta$  strands are predicted to be critical for the mechanical stability of the I1 domain<sup>34</sup> and are highlighted in Figure 1. The high-resolution crystal structure provides an opportunity to examine the mechanical unfolding of proximal Ig domains at atomic details and to compare the mechanical design of proximal and distal Ig domains, which may offer insights into the general principle underlying the mechanical architecture of titin. In addition, Cys37 and Cys62 were found to form a disulfide bridge in the I1 crystal structure, connecting  $\beta$  strands C and E across two  $\beta$ -sheets. This disulfide bridge is different from the classic disulfide bridge found in many extracellular Ig domains, which connects  $\beta$  strands B and F. The disulfide bridge in I1 was proposed to modulate the passive elasticity of titin under oxidative stress. Here, we combine single molecule AFM techniques with protein engineering, to examine the mechanical properties of I1 and test this hypothesis. We constructed a (I27-I1)<sub>4</sub> polyprotein chimera and used single molecule AFM to stretch it to measure its mechanical properties. We found that I1 is mechanically less stable than I27, and that the mechanical unfolding of I1 does not involve an unfolding intermediate state and therefore is an all-or-none event. Through site-directed mutagenesis, we found that the A-B and A'-G patches of the I1 module unravel

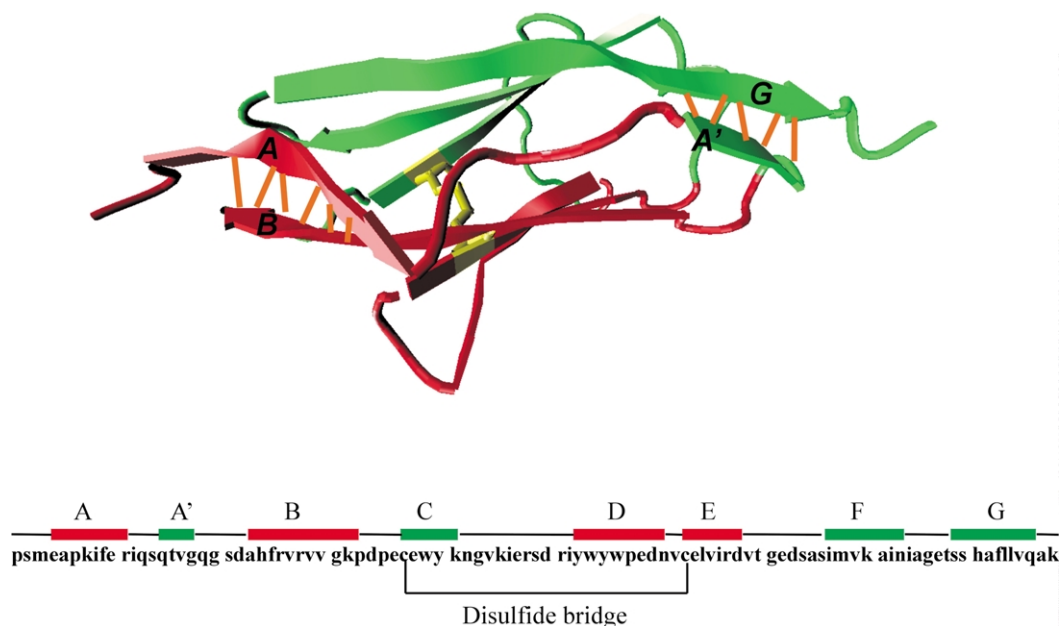


**Figure 1.** The crystal structure and amino acid sequence of the first proximal Ig domain I1 of human cardiac titin. I1 has a characteristic  $\beta$ -sandwich structure with seven antiparallel  $\beta$  strands. A disulfide bridge between Cys37 and Cys62 is present in I1's structure, connecting  $\beta$  strands C and E. This disulfide bridge is highlighted in the structure (yellow bond). Orange bars indicate the backbone hydrogen bonds linking the A and A'  $\beta$  strands to the remainder of I1, which are thought to be critical for the mechanical stability of I1.

together under a mechanical stretching force. This mechanism contrasts that of I27, where the A–B and A'–G patches work independently and break sequentially. In addition, our results show that the formation of the disulfide bridge, found in the I1 crystal structure, is a rare event in aqueous solution, even in an oxidative environment. Our study reveals the mechanical design of a proximal Ig domain, whose features sharply contrast those of distal Ig domains, increasing our understanding on how titin elasticity is finely tuned.

## Results and Discussion

### Mechanical properties of the first proximal Ig domain I1

I1 consists of 100 amino acids and has a characteristic  $\beta$ -sandwich structure with seven antiparallel  $\beta$  strands<sup>33</sup> (Figure 1). We used protein engineering techniques to construct a hetero-polyprotein composed of four tandem repeats of I27-I1 dimer. Here, we used the well-characterized I27 domain from human cardiac titin as a mechanical fingerprint to identify single molecule stretching events.<sup>11,19,24,35</sup> This hetero-polyprotein also allows for a direct comparison of the mechanical properties of I1, a proximal Ig domain with that of I27, a distal Ig domain.

Stretching single (I27-I1)<sub>4</sub> polyprotein chimera results in force–extension curves with a characteristic sawtooth pattern. An example of force–extension curves is shown in Figure 2A. The individual sawtooth corresponds to the mechanical unfolding of individual Ig domains of the stretched polyprotein.<sup>9,21</sup> As the recording shows, there are two clear levels of unfolding forces (dashed lines), one at  $\sim 130$  pN and a second at  $\sim 210$  pN, the latter corresponds to the mechanical unfolding of I27 domains characterized by the mechanical fingerprints of I27 domain unfolding ( $\sim 200$  pN of unfolding forces, and  $\sim 28$  nm in contour length increment, Figure 2A).<sup>21</sup> Since I27 and I1 domains are constructed in an alternating fashion, the low force peaks clearly correspond to the mechanical unfolding of I1 domains in the polyprotein.<sup>19,24</sup> A frequency histogram of unfolding forces of (I27-I1)<sub>4</sub> is plotted in Figure 2B. The histogram shows two separate peaks, centered at  $127(\pm 18)$  pN and  $210(\pm 32)$  pN ( $n = 573$ ), which correspond to the mechanical unfolding of I1 and I27 domains, respectively. This result indicates that I1 is mechanically less stable than I27, in agreement with previous observation that proximal Ig domains are generally less stable than the distal ones.<sup>11,36</sup>

As demonstrated for I27 and other proteins, the mechanical unfolding of proteins is typically a non-equilibrium process, therefore the force required to unfold a protein module depends on the pulling speed. Figure 2C plots the pulling speed dependence for the two levels of unfolding

forces observed for (I27-I1)<sub>4</sub> polyprotein. We used Monte Carlo simulation<sup>21</sup> to estimate the mechanical unfolding rate constant at zero force and the distance to the transition state by simultaneously predicting the distribution of unfolding force at a given pulling speed (Figure 2B) and the speed dependence of unfolding forces (Figure 2C). The distribution of unfolding forces are predicted by the Monte Carlo simulations using unfolding rate constants at zero force,  $k_u^0$ , of  $5.0 \times 10^{-3} \text{ s}^{-1}$  for I1 and  $3.3 \times 10^{-4} \text{ s}^{-1}$  for I27 (Figure 2B and C, solid lines). The unfolding distance to the transition state is  $\Delta x_u = 0.35$  nm for I1 and  $\Delta x_u = 0.25$  nm for I27, respectively. However, as demonstrated before,<sup>21,37</sup> these numbers can only be viewed as estimates, as the use of Monte Carlo simulations to estimate these parameters has a low sensitivity.

In addition to the different mechanical stability, I1 and I27 also show a difference in contour length increment ( $\Delta L_c$ ) observed upon domain unfolding. We used the worm-like-chain (WLC) model<sup>38</sup> of polymer elasticity to fit consecutive force peaks and estimate the contour length increment upon domain unfolding (Figures 2A and 3A, red solid lines). The measured contour length increment for I1 and I27 are plotted in the frequency histogram shown in Figure 3B for I1 and Figure 3C for I27 domain, respectively. A Gaussian fit of the I27 distribution (red line, Figure 3C) measures  $\Delta L_c = 27.9(\pm 0.79)$  nm. In contrast, a Gaussian fit of the I1 distribution (red line, Figure 3B) measures  $\Delta L_c = 30.0(\pm 0.62)$  nm, which is longer than that of the I27 domain and of the other proximal Ig domains, such as I4 and I5.<sup>11</sup> I1 is 100 amino acid long and has a folded length of  $\sim 5.6$  nm.<sup>33</sup> Hence, a complete unfolding of I1 domain should result in a length increment of 30.4 nm assuming a peptide length of 0.36 nm<sup>39</sup> ( $0.36 \text{ nm/aa} \times 100\text{aa} = 5.6 \text{ nm}$ ), in excellent agreement with our measurements.

In the vast majority ( $>94\%$ ,  $n = 295$ ) of force–extension curves of (I27-I1)<sub>4</sub>, the unfolding of the I1 domains is accompanied by a contour length increment of  $\sim 30$  nm. However, in rare cases ( $<6\%$ ), we also observed force–extension curves showing two different spacing (Figure 3A): in addition to contour length increases in  $\Delta L_c \sim 30$  nm (as indicated by red arrows), these force–extension curves also show events with a much shorter contour length increment, as indicated by blue arrows in Figure 3A. WLC fits to these events resulted in a minor peak in the  $\Delta L_c$  histogram for I1 (Figure 3B). A Gaussian fit measures a contour length increase in  $\Delta L_c = 21.7(\pm 1.28)$  nm for these events, which is 8.3 nm shorter than the contour length increment that resulted from a complete unfolding of an I1 domain. This result suggests that, after the I1 domain unfolding, about 23 amino acids (8.3 nm/0.36 nm) remain “hidden” from the stretching force in the unfolded state and are therefore “short-circuited” by a putative unbreakable bond.

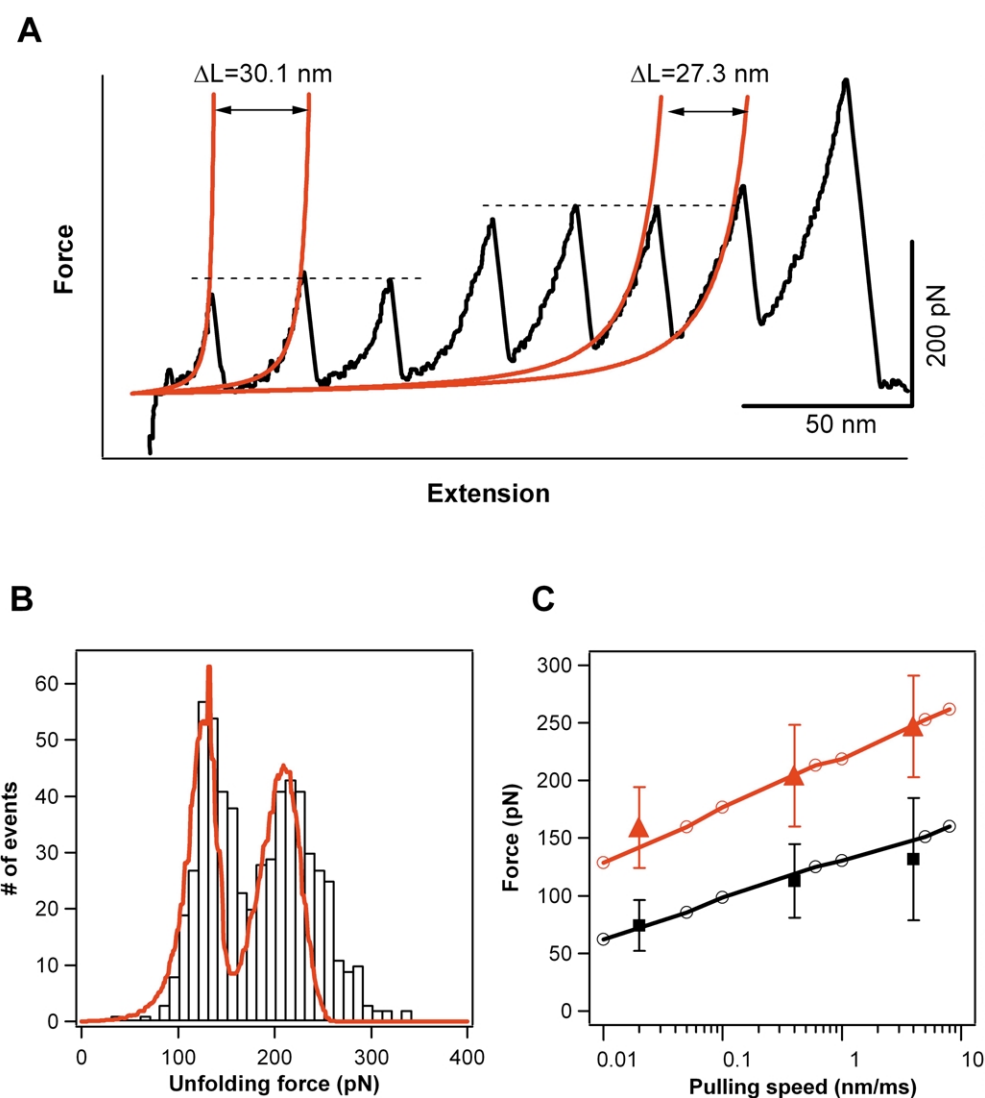


**Figure 2.** Mechanical properties of the first proximal Ig domain I1. **A**, A typical force–extension curve of a polyprotein chimera (I27-I1)<sub>4</sub>. The well-characterized I27 domains are used as a mechanical fingerprint to identify the stretching and unfolding of I1 domains. The force–extension curves show two distinct levels of unfolding forces (dashed lines), one at ~130 pN with a contour length increment of ~30 nm; a second at ~210 pN with a contour length increment of ~28 nm, the latter corresponds to the unfolding of I27 domains. **B**, Histogram of the unfolding forces for the (I27-I1)<sub>4</sub> polyprotein. There are two clearly separated peaks, one at 127 pN and a second at 211 pN ( $n = 595$ ). The line corresponds to Monte Carlo simulations of the unfolding forces of (I27-I1)<sub>4</sub> polyprotein (1000 trials). The unfolding rate constants at zero force we used in Monte Carlo simulations were:  $k_u^0 = 5.0 \times 10^{-3} \text{ s}^{-1}$  for I1 domains,  $k_u^0 = 3.3 \times 10^{-4} \text{ s}^{-1}$  for I27 domains. The unfolding distance was assumed to be  $\Delta x_u = 0.35 \text{ nm}$  for I1 domains and  $\Delta x_u = 0.25 \text{ nm}$  for I27 domains, respectively. **C**, Plot of pulling speed dependence for two levels of unfolding forces observed for (I27-I1)<sub>4</sub> polyprotein chimera. Open circles, connected by solid lines, correspond to Monte Carlo simulations at seven different pulling speeds (30 trials at each pulling speed). The parameters used in Monte Carlo simulations are same as those listed in **B**.

The X-ray crystal structure of I1 revealed a disulfide bridge in the  $\beta$ -sandwich structure, connecting Cys37 (located on  $\beta$  strand C) and Cys62 (located on  $\beta$  strand E).<sup>33</sup> This disulfide bridge is formed under ambient condition during crystallization process, readily oxidized by ambient O<sub>2</sub>. It has been demonstrated that disulfide bonds are mechanically very stable, requiring ~1.4 nN to break.<sup>40</sup> Hence, under our typical experimental condition, an S–S bond will

remain intact under a stretching force, predicting that the 26 amino acids between Cys37 and Cys62 will be locked upon formation of a disulfide bridge, limiting the extensibility of the I1 polypeptide chain. Steered molecular dynamics (SMD) simulation of the mechanical unfolding of the I1 domain in the presence of a disulfide bridge<sup>34</sup> also suggested that formation of the disulfide bond limits the extensibility of the I1 domain and the unfolded I1 domain could only extend by

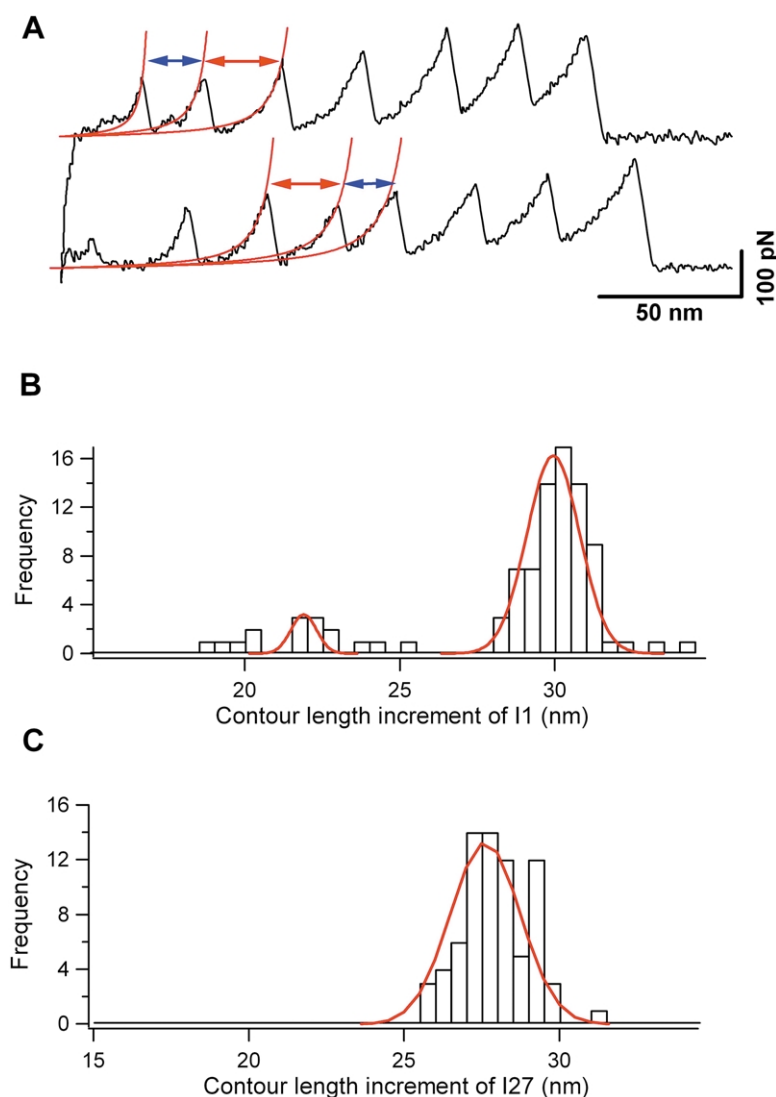


**Figure 3.** I1 and I27 domains show different contour length increment upon domain unfolding. A, Force-extension curves of (I27-I1)<sub>4</sub> polyproteins. In single molecule AFM experiments, the vast majority of force-extension curves (>94%) of (I27-I1)<sub>4</sub> we observed are similar to those shown in Figure 2A, in which I1 domains show contour length increments of ~30 nm corresponding to the complete unraveling of I1 domain; in rare cases, we observed force-extension curves in which I1 shows contour length increments between 18 nm and 24 nm (as indicated by the blue arrows), in addition to the regular 30 nm in contour length increment (as indicated by the red arrows). B, Histogram of contour length increments of the I1 domains shows a bimodal distribution: one at 30.0 nm and a second one at 21.7 nm. The contour length increment of 30 nm corresponds to the unraveling of the reduced I1 domains, whereas the contour length increment of 21.9 nm corresponds to the unraveling of the oxidized I1 domains which contain a disulfide bridge. C, Histogram of contour length increment of I27 domains shows a peak at 27.9 nm. Red lines in B and C are Gaussian fits to the measured contour length increment frequency histograms.

~22 nm, in excellent agreement with our experimental findings. This suggests that, in our AFM studies, the observed force peak spacing of ~22 nm (Figure 3A and B) corresponds to the mechanical unfolding of I1 domains with a disulfide bridge, while the spacing of 30 nm corresponds to the complete unfolding of the reduced form of the I1 domains in which no disulfide bridge is present. Stretching the (I27-I1)<sub>4</sub> polyprotein in the presence of 50 mM dithiothreitol (DTT), a strong reagent to reduce the disulfide bridge, further confirms our interpretation. When stretched in the presence of DTT, all I1 domains unfold with a contour length increment of ~30 nm, corresponding to the complete unraveling of I1 domains which are in the reduced state. Under these conditions, no force peak spacing of ~22 nm was observed in over 100 I1 domain unfolding events (data not shown). Our (I27-I1)<sub>4</sub> polyproteins are stored at 4 °C and at pH 7.4, it is likely that the oxidation, which leads to the formation of a disulfide bridge, is due to the ambient O<sub>2</sub>. However, the extremely low

population of the oxidized I1 form suggests that the oxidation reaction is highly unfavorable under our experimental conditions.

### The mechanical unfolding of I1 is an all-or-none event

Previously we have shown that the mechanical unfolding of the distal Ig domains, such as I27, I28 and I32, go through an unfolding intermediate state, which plays an important role in stabilizing the distal Ig domains.<sup>11,12</sup> The unfolding intermediate state manifests itself as a “hump” in the force-extension curve, which clearly deviates from the WLC model of polymer elasticity. This feature is again evident for the unfolding events of I27 domains in the force-extension curve of (I27-I1)<sub>4</sub> polyprotein, shown in Figure 4. WLC fits (thin lines, Figure 4) to the unfolding event of I27 measure a length increase in 0.8 nm/module upon I27 undergoing a transition from the native state to the unfolding intermediate state, in agreement

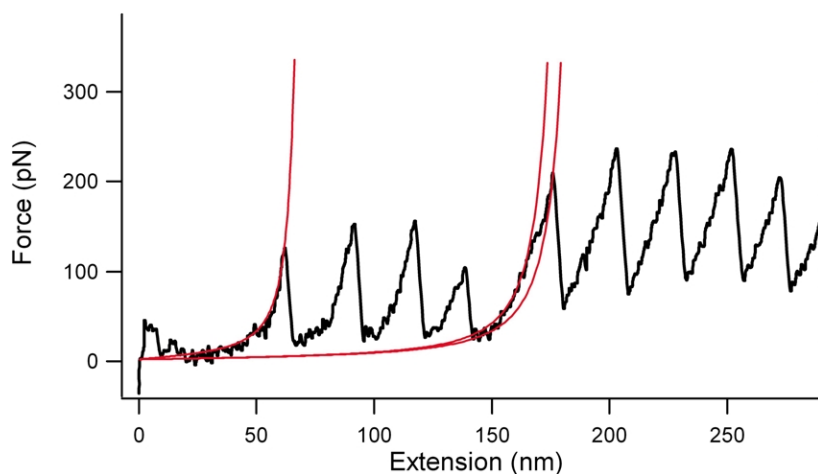


**Figure 4.** The mechanical unfolding of the I1 domains is an all-or-none event. The black trace is a force–extension curve of (I27–I1)<sub>4</sub>, red lines are WLC fits to the experimental data. The force–extension relationship for the unfolding of I27 domains shows a clear hump, which deviates from the WLC fit. This hump has been identified as an unfolding intermediate state prior to the main unfolding event of I27. In contrast to the I27 domains, the I1 domains do not show a “hump” prior to the main unfolding event and the force–extension relationship of I1 can be well-described by the WLC model, indicating that no unfolding intermediate state can be detected along the mechanical unfolding pathway of the I1 domain.

with our previous measurements carried out on (I27)<sub>12</sub> homopolyproteins.<sup>12</sup>

In contrast to I27, the force–extension curves for I1 are well described by the WLC model, no deviation from the WLC model can be detected within the experimental error (Figure 4). This result suggests that there is no similar unfolding intermediate state along the mechanical unfolding pathway of I1. Therefore, the mechanical unfolding of I1 under these conditions is apparently an all-or-none event. This finding is consistent with our previous observations on other proximal Ig domains,<sup>11</sup> indicating that the lack of an unfolding intermediate preceding the main unfolding event may be a general feature of the proximal Ig domains of titin. Although the I1 domain does not show any unfolding intermediate state similar to that of the I27 domain in force–extension measurements, we cannot rule out the possibility that unfolding intermediate states may exist after the main unfolding event or appear under a different set of experimental conditions. For example, the intermediate state in I27 occurs before the main unfolding event, therefore it is easy to detect in our AFM experiments.<sup>11,12</sup> However, if an intermediate state existed after the main unfolding event, as predicted for the FnIII domains,<sup>41,42</sup> it could be hidden by the cantilever backlash and invisible in AFM force–extension recordings.

### Molecular basis of the mechanical unfolding of I1

I1 and I27 share similar  $\beta$ -sandwich structure. Both have seven anti-parallel  $\beta$  strands that are arranged into two  $\beta$  sheets packing against each other (Figure 1).<sup>26,33</sup> It has been predicated by SMD simulation that the backbone hydrogen bonds attaching the A' and A  $\beta$ -strands to the remainder of the fold are critical in maintaining

the mechanical integrity of the protein.<sup>25,27</sup> In addition, single molecule AFM experiments suggested that other non-covalent interactions, such as hydrophobic interaction, may also contribute to the overall mechanical stability of a protein module.<sup>23</sup> The major difference between I1 and I27 is the number of backbone hydrogen bonds and their distribution in these two regions: I1 has more backbone hydrogen bonds between its A- and B- $\beta$  strands than those between the A' and G strands (six *versus* five), while I27 is the opposite (two backbone hydrogen bonds between A and B  $\beta$  strands *versus* six between its A' and G  $\beta$  strands).

SMD simulation and other modeling approaches of mechanical unfolding of proteins have provided invaluable atomic description of the key events leading to its mechanical unfolding.<sup>12,25,27,30,32</sup> SMD simulation of the mechanical unfolding of I27 showed that two backbone hydrogen bonds between A- and B- $\beta$  strands break first, resulting in an unfolding intermediate state. The subsequent unraveling of the A–G' patch triggers the complete unfolding of the I27 domain. In contrast to the three-state unfolding of the I27 domain, our own SMD data<sup>11</sup> and that of Schulten *et al.*<sup>34</sup> on I1 have shown that the A–B and A'–G patches in the I1 domain unravel together. After the unraveling and separation of both the A–B and A'–G patches, the remainder of I1 will unravel without significant energy barriers. This result provides a molecular mechanism under which I1 can unfold without a significant unfolding intermediate in an all-or-none fashion.

SMD simulations showed that the unfolding event of the I1 domain coincides with the rupture of backbone hydrogen bonds between A–B  $\beta$  strands and between A'–G  $\beta$  strands. In order to examine the role of the A–B and A'–G  $\beta$  strands in the mechanical stability of I1, we used

site-directed mutagenesis to introduce proline residues into the A–B and A'–G patches. The positions of the I1 mutations were chosen to block the formation of selected backbone hydrogen bonds in the A–B and A'–G regions of the protein rather than to be in the exact same positions of those in I27. In addition to disrupting hydrogen bonds, proline mutations are likely to disrupt local  $\beta$ -sheet structure and affect other non-covalent interactions in the mutated regions.<sup>43</sup> We

constructed five different (I27-I1)<sub>4</sub> polyproteins containing point mutation in the A–B patch (I1-E4P, K7P and R28P) and in the A'–G patch (I1-Q15P and V17P) of the I1 domain, and used single molecule AFM to measure the effect of these mutations on the mechanical stability of I1 (Figure 5A). Mutants Q15P and V17P of I1 happen to be in the same positions as the mutants V11P and V13P of I27, while E4P, K7P and R28P in I1 are in different positions (see sequence alignments<sup>33,34</sup>).

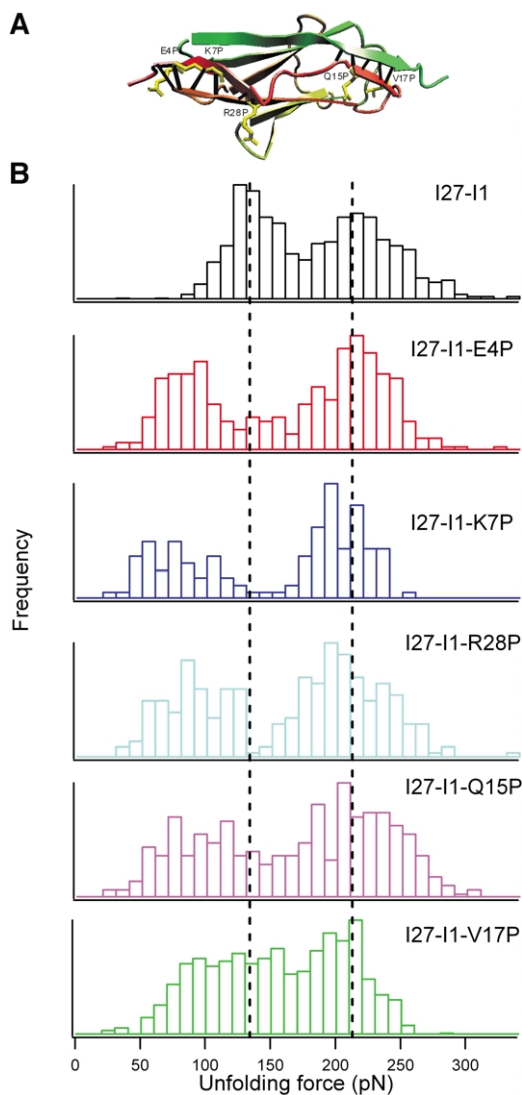


**Figure 5.** Mechanical properties of the I1 mutants. A, A cartoon shows the  $\beta$ -sandwich structure of the I1 module and the amino acids that are substituted by prolines in this work. Black bars indicate the six backbone hydrogen bonds linking the A and B  $\beta$  strands and five backbone hydrogen bonds linking the A' and G  $\beta$  strands. B, The unfolding force histogram of I27-I1 mutant polyproteins: I27-I1 wt (black), I27-I1-E4P (red), I27-I1-K7P (blue), I27-I1-R28P (cyan), I27-I1-Q15P (purple) and I27-I1-V17P (green). All the histograms show two distinct unfolding force peaks. The unfolding force of I27 remains the same for all the constructs, while the unfolding forces of I1 mutants decrease compared with that of I1 wt.

### Mechanical topology and unfolding pathway of I1

Figure 5B compares the unfolding force distribution of the wild-type polyprotein and five mutants. As expected, the unfolding forces of the fingerprint I27 domains remain the same in all constructs ( $\sim 200$  pN). However, I1 mutants E4P, K7P, Q15P, V17P and R28P show reduced unfolding forces (E4P,  $80(\pm 23)$  pN,  $n = 300$ ; K7P,  $69(\pm 30)$  pN,  $n = 119$ ; R28P,  $82(\pm 28)$  pN,  $n = 238$ ; Q15P,  $82(\pm 28)$  pN,  $n = 337$ ; V17P,  $117(\pm 42)$  pN,  $n = 543$ ; average forces given) as compared to the wild-type I1 protein ( $127(\pm 18)$  pN,  $n = 595$ ) (Figure 2B). This result demonstrates that the removal of backbone hydrogen bonds and local structural disruption in the A–B and A'–G patches mechanically weaken the I1 module, indicating that all these residues are important in maintaining the mechanical integrity of I1. The proline mutants in the A–B patch (I1-E4P, I1-K7P and I1-R28P) have a significant destabilizing effect on the mechanical properties of I1. The unfolding forces for these mutant proteins drop by more than 40% compared with that of the wild-type. This contrast the results obtained for the I27 domain, where a proline mutation in the A–B patch left the main unfolding peaks unchanged, while its main effect was the elimination of the intermediate state.

We have shown that the unfolding force of a module depends on the pulling speed. From the speed dependence of unfolding forces one can estimate the distance to the transition state and unfolding rate constant at zero force. Here, we carried out single molecule stretching experiment at different pulling speeds and determined these two parameters for the unfolding of E4P and V17P mutants (Figure 6). We found that E4P and V17P mutants show similar speed dependence as the wild-type, suggesting that I1 mutants and wild-type have a similar distance to the transition state. Using the Monte Carlo approach,<sup>21,37</sup> we estimate the distance to the transition state of I1 mutants to be 0.35 nm. We also estimated the unfolding rate constant of I1 mutants at zero force: E4P:  $\alpha_0 = 7 \times 10^{-2} \text{ s}^{-1}$ ,  $\Delta x_u = 0.35 \text{ nm}$ ; K7P:  $\alpha_0 = 0.1 \text{ s}^{-1}$ ,  $\Delta x_u = 0.35 \text{ nm}$ ; R28P:  $\alpha_0 = 5 \times 10^{-2} \text{ s}^{-1}$ ,  $\Delta x_u = 0.35 \text{ nm}$ ; Q15P:  $\alpha_0 = 5 \times 10^{-2} \text{ s}^{-1}$ ,  $\Delta x_u = 0.35 \text{ nm}$ ; V17P:  $\alpha_0 = 8 \times 10^{-3} \text{ s}^{-1}$ ,  $\Delta x_u = 0.35 \text{ nm}$ . These results suggest that the proline mutations

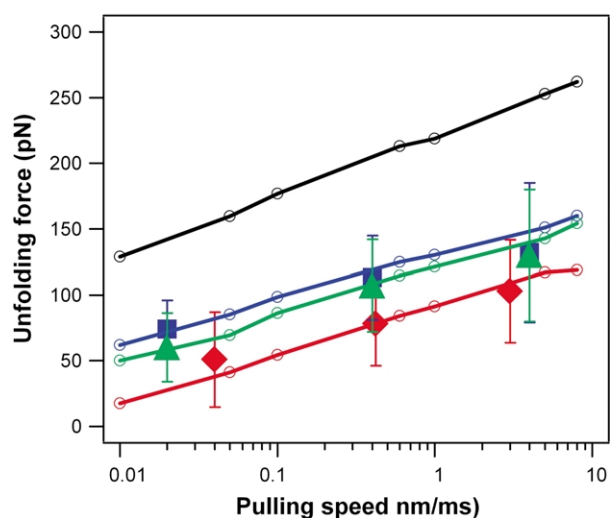


**Figure 6.** A plot of average unfolding force *versus* pulling speed reveals the phenotypical effect of proline mutations on the mechanical properties of the I1 domain. The experimental data are shown as squares for I1-wt, diamonds for I1-E4P and triangles for I1-V17P. Open circles, connected by solid lines, correspond to Monte Carlo simulation results: I1-wt (blue), I1-E4P (red) and I1-V17P (green). For comparison, the Monte Carlo simulation of the speed dependence of the unfolding forces for the I27 domains is also shown here (black line). Parameters used in Monte Carlo simulations are listed in the main text. Monte Carlo simulations were performed at seven different pulling speeds with 30 trials at each speed.

destabilize the I1 domain by lowering its unfolding energy barrier, while the transition state and unfolding pathway remain the same for the I1 mutants. This contrasts the phenotypic effects of proline mutations in I27 domain. For I27 domain, proline mutations in the A'-G region decreased the unfolding forces required to unravel I27 domain and increased the distance from the native state to the transition state.<sup>23,37</sup> The difference in the phenotypic effect of proline mutation in similar region of I1 and I27 domains again showed the substantial difference in the mechanical unfolding energy landscapes for both domains.

Our results confirm the prediction made by SMD simulations, that the major mechanical resistance of I1 arises from the A-B and A'-G patches.<sup>34</sup> In addition, our results also reveal the close connection between A-B and A'-G patches, where a disruptive proline mutation in either A-B or A'-G patch has a destabilizing effect on the overall mechanical stability. This result indicates that, unlike the I27 module, the A-B and A'-G patches are mechanically coupled. The mechanical coupling allows the A-B and A'-G patches to work in a cooperative manner to provide the mechanical resistance to the I1 domain. This mechanical design is very different from that of I27. For the I27 domain, the A-B and A'-G patches behave independently of each other. A mutation in

the A-B patch changed the properties of the unfolding intermediate, which corresponds to the separation of the A-B patch, but has no effect on the main energy barrier to unfolding, which corresponds to the unraveling of the A'-G patch.<sup>12</sup>

### The mechanical stability of the I1 domain affects the formation of the disulfide bridge

In addition to destabilizing effects on the mechanical stability, proline substitutions in the A-B and A'-G patches also have important effects on the formation of the disulfide bridge. In contrast to the rare occurrence of a disulfide bridge in wild-type I1, the I1 mutants E4P, K7P Q15P and R28P more readily show the formation of the disulfide bridge. Force-extension curves of these mutants frequently show mixed spacing, as illustrated by the WLC fits to the data shown in Figure 7 (left panel). One type of force peak spacing is the standard  $\sim 30$  nm (red arrows) corresponding to the unraveling of the reduced form. The other type of force peak spacing is  $\sim 22$  nm (blue arrows) corresponding to the unraveling of the oxidized form of I1. In a few cases, we have observed that the mutant I1 modules of a polyprotein all appear in the oxidized form. Histograms of the contour length increment upon I1 domain unfolding were plotted in Figure 7 (right panel). The force peak spacing for the mutant proteins E4P, K7P Q15P and R28P show a clear bimodal distribution, with the first peak centered at  $\sim 22$  nm and the second peak centered at  $\sim 30$  nm. In contrast, the mutant V17P shows mainly one dominant peak at  $\sim 30$  nm. The bimodal distribution of the force peak spacing for the mutants (E4P, K7P, V15P and R28P) shows that the equilibrium between the oxidized and reduced forms of I1 shifted significantly towards the oxidized form. In contrast to the low count of the oxidized form in the wild-type ( $<6\%$ ) and the mutant V17P ( $\sim 7\%$ ,  $n = 98$ ), the total counts of the oxidized form significantly increase in the mutant I1 proteins (E4P: 40%,  $n = 106$ ; K7P: 64%,  $n = 28$ ; Q15P: 60%,  $n = 48$ ; R28P: 50%,  $n = 34$ ). However, it is rare to observe force-extension recordings where all the I1 domains in a single sawtooth pattern are in the oxidized form. Mostly, in any given recording we observed mixtures of oxidized and reduced I1 unfolding events.

The mutants E4P, K7P, R28P and Q15P show significant decreases in mechanical stability and a corresponding increase in unfolding rate constant at zero force, while the mutant V17P and the wild-type have a much higher mechanical stability and a smaller unfolding rate constant. The correlation, between the mechanical stability of I1 and the ease to form a disulfide bridge, suggests that the mechanical weakening of I1 domains facilitates the formation of the disulfide bridge. Two possible factors may contribute to this effect. One is the structural flexibility of the region involving two

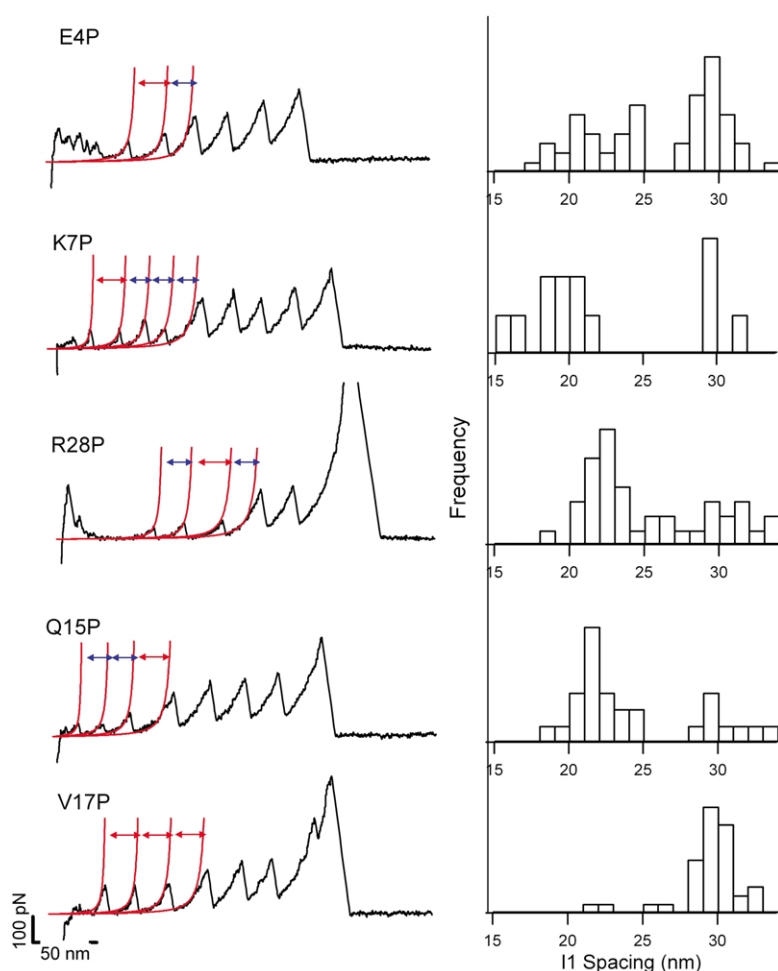


**Figure 7.** Proline mutation facilitates the formation of a disulfide bridge. Left panel shows the force–extension curve of the I1 proline mutants. The red lines correspond to the WLC fits to the experimental data. Fits demonstrate that the mutant E4P, K7P, R28P and Q15P have two different contour length increments: one is  $\sim 30$  nm as indicated by the red arrows; a second one is  $\sim 22$  nm as indicated by blue arrows. Mutant V17P predominantly shows one type of force peak spacing which is  $\sim 30$  nm. Right panel shows the force peak spacing histograms observed for I1 mutants. E4P, K7P, Q15P and R28P show bimodal distribution in force peak spacing, one peak centered at  $\sim 22$  nm, the other one at  $\sim 30$  nm. The bimodal distribution indicates that these mutants exist in equilibrium between two populations: reduced and oxidized forms. V17P is similar to the wild-type and predominantly exists in the reduced form.

cysteine residues. Previous studies<sup>33</sup> have shown that the disulfide bridge forms only after the domain folds into its compact  $\beta$ -sandwich structure; this is in contrast to most extracellular disulfide bridged proteins where the formation of disulfide bridge is critical for the correct folding of proteins.<sup>44</sup> The rigidity of the  $\beta$ -sheet structure in I1 may hinder the formation of the disulfide bond. It is possible that the local disruption caused by proline mutation confers enough flexibility to this region, allowing the disulfide bridge to form. The second factor may be the accessibility of cysteine residues to  $O_2$ . The cysteine residues in the I1 domain are buried inside the hydrophobic core. The compact packing of the  $\beta$ -sandwich structure may prevent  $O_2$  from accessing the cysteine residues. A local disruption of the  $\beta$ -sandwich may increase the accessibility of molecular  $O_2$  to the two cysteine residues buried in the hydrophobic core. The combined effect of increasing flexibility and accessibility to  $O_2$  may facilitate the formation of the disulfide bridge in I1.

Since the intracellular environment, where titin performs its physiological functions, is considered to be reducing, it is most unlikely that a disulfide bridge will form in I1 and plays physiological roles in titin elasticity.<sup>33</sup> Prompted by the

unexpected finding of a disulfide bridge in the I1 crystal structure, Willmans and colleagues carried out sequence analysis of titin and predicted that 40 out of 92 I band Ig domains contain appropriate cysteine pattern which have the potential of forming disulfide bridges under oxidative stress.<sup>33</sup> They proposed a mechanism in which reversible formation of a disulfide bridges could regulate the extensibility of I band titin.<sup>33</sup> However, our results do not support this mechanism. Our results strongly suggest that the formation of a disulfide bridge in I1 is unlikely in aqueous solution even in an oxidative environment. SMD simulation provides additional evidence to support our conclusion. After equilibration in water for 1 ns, the structure of the oxidized I1 shows that, the distances between the two sulfur atoms ( $S-S$ ) and between the two  $\beta$  carbon atoms ( $C^\beta-C^\beta$ ) of the two cysteine residues (Cys37 and Cys62) are  $\sim 2.0$  Å and 3.8 Å respectively (K. Schulten & M. Gao, personal communication). In contrast, after equilibration in water for 1 ns, the structure of the reduced I1 shows that the  $S-S$  and  $C^\beta-C^\beta$  distances increased to 3.8 Å and 4.8 Å, respectively. It has been shown that the  $C^\beta-C^\beta$  distance required to form a disulfide bridge is in the range of 3.45–4.5 Å.<sup>45</sup> The  $C^\beta-C^\beta$  distance in the reduced I1

domain is beyond the optimum range for a disulfide bridge to form. From the modeling point of view, it is therefore intrinsically unfavorable for the two cysteine residues in I1 to form a disulfide bridge in aqueous solution; this agrees well with our observations on I1. The observation of a disulfide bridge in the crystal structure may have resulted from the unique condition imposed by the crystal packing. However, a thorough SMD simulation is needed to elaborate this point and will be the subject of a future publication.

The present study confirms the critical importance of the A–B and A'–G patches of Ig domains in providing for their mechanical resistance. Although I1 and I27 domains share similar structure, they have distinct mechanical properties. Subtle structural differences such as the distribution of the backbone hydrogen bonds, hydrophobic interactions and salt bridges determine the mechanical properties of the resulting protein domains. This is one of the most important features of the mechanical design of the I-band titin. Considering the enormous size of titin and the importance of muscle passive elasticity to physiology, it is intriguing that only a small number of A–B and A'–G patches-like motifs could determine the mechanical properties of the elastic Ig regions of titin. Therefore, it is possible that A–B and A'–G patches may function as "mechanical active sites" in titin mechanics, similar to the active sites of enzyme catalysis. Perhaps Nature has selectively focused evolutionary pressure on these "active sites", instead of the whole titin sequence, to optimize the mechanical properties of titin and therefore the performance of different muscles types.

## Materials and Methods

### Protein engineering

We constructed polyprotein chimeras that contained four direct tandem repeats of an I27-I1 dimer or I27-I1 mutant dimer ((I27-I1)<sub>4</sub>, (I27-I1-E4P)<sub>4</sub>, (I27-I1-K7P)<sub>4</sub>, (I27-I1-Q15P)<sub>4</sub>, (I27-I1-V17P)<sub>4</sub>, and (I27-I1-R28P)<sub>4</sub>). I27 and I1 monomers were amplified from a human cardiac muscle cDNA clone using polymerase-chain-reaction. Point mutations were introduced to I1 monomer using a Quick-change mutagenesis kit from Qiagen. I27, I1 and I1 mutant monomers were flanked with a 5' *Bam*HI restriction site and 3' *Bgl*II, *Kpn*I restriction sites. Polyprotein DNA were constructed using a previously described method<sup>21</sup> based on the identity of the sticky ends generated by *Bam*HI and *Bgl*II restriction enzymes and subcloned into a modified pET-blue expression vector. All polyproteins were expressed in *E. coli* pLacBL(DE3)-tuner strain (Qiagen). Proteins were purified by Ni<sup>2+</sup>-affinity chromatography followed by additional size-exclusion FPLC purification step. Proteins were kept at 4 °C in Tris/NaCl at pH 8.4. All the constructs used in this study have a His-tag at the N terminus for affinity purification, and two Cys codons at the C terminus to facilitate the covalent attachment of polyproteins to the gold substrate through the Au–S bond.

### Single molecule atomic force microscopy

Single-molecule AFM has been described in detail<sup>46–48</sup> elsewhere. Force–extension measurements were carried out in PBS buffer. The cantilevers are standard Si<sub>3</sub>N<sub>4</sub> cantilevers with a typical spring constant of ~40 pN/nm. (ThermoMicroscope, Sunnyvale, CA). Every cantilever was calibrated in solution using the equipartition theorem. Unless noted in the text, the pulling speed of all force–extension curves was in the range of 0.4–0.6 nm/ms.

## Acknowledgements

We thank J. Kerkvliet for his help in polyprotein engineering, M. Gao and K. Schulten for sharing SMD simulation trajectories of the I1 domain, L. Li and A. Sarkar for helpful discussion. This work is supported by National Institutes of Health grant to J.M.F.

## References

1. Wang, K. (1996). Titin/connectin and nebulin: giant protein rulers of muscle structure and function. *Advan. Biophys.* **33**, 123–134.
2. Maruyama, K. (1997). Connectin/titin, giant elastic protein of muscle. *FASEB J.* **11**, 341–345.
3. Labeit, S. & Kolmerer, B. (1995). Titins: giant proteins in charge of muscle ultrastructure and elasticity. *Science*, **270**, 293–296.
4. Brady, A. J. (1991). Mechanical properties of isolated cardiac myocytes. *Physiol. Rev.* **71**, 413–428.
5. Trinick, J. (1996). Titin as a scaffold and spring. Cytoskeleton. *Curr. Biol.* **6**, 258–260.
6. Tskhovrebova, L. & Trinick, J. (2002). Role of titin in vertebrate striated muscle. *Philos. Trans. Roy. Soc. ser. B. Biol. Sci.* **357**, 199–206.
7. Labeit, S., Kolmerer, B. & Linke, W. A. (1997). The giant protein titin. Emerging roles in physiology and pathophysiology. *Circ. Res.* **80**, 290–294.
8. Kellermayer, M. S., Smith, S. B., Granzier, H. L. & Bustamante, C. (1997). Folding–unfolding transitions in single titin molecules characterized with laser tweezers. *Science*, **276**, 1112–1116.
9. Rief, M., Gautel, M., Oesterhelt, F., Fernandez, J. M. & Gaub, H. E. (1997). Reversible unfolding of individual titin immunoglobulin domains by AFM. *Science*, **276**, 1109–1112.
10. Erickson, H. P. (1997). Stretching single protein molecules: titin is a weird spring. *Science*, **276**, 1090–1092.
11. Li, H., Linke, W. A., Oberhauser, A. F., Carrion-Vazquez, M., Kerkvliet, J. G., Lu, H. *et al.* (2002). Reverse engineering of the giant muscle protein titin. *Nature*, **418**, 998–1002.
12. Marszalek, P. E., Lu, H., Li, H., Carrion-Vazquez, M., Oberhauser, A. F., Schulten, K. & Fernandez, J. M. (1999). Mechanical unfolding intermediates in titin modules. *Nature*, **402**, 100–103.
13. Tskhovrebova, L., Trinick, J., Sleep, J. A. & Simmons, R. M. (1997). Elasticity and unfolding of single molecules of the giant muscle protein titin. *Nature*, **387**, 308–312.

14. Linke, W. A., Rudy, D. E., Centner, T., Gautel, M., Witt, C., Labeit, S. & Gregorio, C. C. (1999). I-band titin in cardiac muscle is a three-element molecular spring and is critical for maintaining thin filament structure. *J. Cell. Biol.* **146**, 631–644.
15. Bang, M. L., Centner, T., Fornoff, F., Geach, A. J., Gotthardt, M., McNabb, M. *et al.* (2001). The complete gene sequence of titin, expression of an unusual approximately 700-kDa titin isoform, and its interaction with obscurin identify a novel Z-line to I-band linking system. *Circ. Res.* **89**, 1065–1072.
16. Witt, C. C., Olivieri, N., Centner, T., Kolmerer, B., Millevoi, S., Morell, J. *et al.* (1998). A survey of the primary structure and the interspecies conservation of I-band titin's elastic elements in vertebrates. *J. Struct. Biol.* **122**, 206–215.
17. Politou, A. S., Thomas, D. J. & Pastore, A. (1995). The folding and stability of titin immunoglobulin-like modules, with implications for the mechanism of elasticity. *Biophys. J.* **69**, 2601–2610.
18. Trombitas, K., Freiburg, A., Centner, T., Labeit, S. & Granzier, H. (1999). Molecular dissection of N2B cardiac titin's extensibility. *Biophys. J.* **77**, 3189–3196.
19. Li, H., Oberhauser, A. F., Redick, S. D., Carrion-Vazquez, M., Erickson, H. P. & Fernandez, J. M. (2001). Multiple conformations of PEVK proteins detected by single-molecule techniques. *Proc. Natl Acad. Sci. USA*, **98**, 10682–10686.
20. Watanabe, K., Nair, P., Labeit, D., Kellermayer, M. S., Greaser, M., Labeit, S. & Granzier, H. (2002). Molecular mechanics of cardiac titin's PEVK and N2B spring elements. *J. Biol. Chem.* **277**, 11549–11558.
21. Carrion-Vazquez, M., Oberhauser, A. F., Fowler, S. B., Marszalek, P. E., Broedel, S. E., Clarke, J. & Fernandez, J. M. (1999). Mechanical and chemical unfolding of a single protein: a comparison. *Proc. Natl Acad. Sci. USA*, **96**, 3694–3699.
22. Carrion-Vazquez, M., Marszalek, P. E., Oberhauser, A. F. & Fernandez, J. M. (1999). Atomic force microscopy captures length phenotypes in single proteins. *Proc. Natl Acad. Sci. USA*, **96**, 11288–11292.
23. Li, H., Carrion-Vazquez, M., Oberhauser, A. F., Marszalek, P. E. & Fernandez, J. M. (2000). Point mutations alter the mechanical stability of immunoglobulin modules. *Nature Struct. Biol.* **7**, 1117–1120.
24. Li, H., Oberhauser, A. F., Fowler, S. B., Clarke, J. & Fernandez, J. M. (2000). Atomic force microscopy reveals the mechanical design of a modular protein. *Proc. Natl Acad. Sci. USA*, **97**, 6527–6531.
25. Lu, H. & Schulten, K. (2000). The key event in force-induced unfolding of Titin's immunoglobulin domains. *Biophys. J.* **79**, 51–65.
26. Improta, S., Politou, A. S. & Pastore, A. (1996). Immunoglobulin-like modules from titin I-band: extensible components of muscle elasticity. *Structure*, **4**, 323–337.
27. Lu, H., Isralewitz, B., Krammer, A., Vogel, V. & Schulten, K. (1998). Unfolding of titin immunoglobulin domains by steered molecular dynamics simulation. *Biophys. J.* **75**, 662–671.
28. Brockwell, D. J., Beddard, G. S., Clarkson, J., Zinober, R. C., Blake, A. W., Trinick, J. *et al.* (2002). The effect of core destabilization on the mechanical resistance of I27. *Biophys. J.* **83**, 458–472.
29. Fowler, S. B., Best, R. B., Toca Herrera, J. L., Rutherford, T. J., Steward, A., Paci, E. *et al.* (2002). Mechanical unfolding of a titin Ig domain: structure of unfolding intermediate revealed by combining AFM, molecular dynamics simulations, NMR and protein engineering. *J. Mol. Biol.* **322**, 841–849.
30. Paci, E. & Karplus, M. (2000). Unfolding proteins by external forces and temperature: the importance of topology and energetics. *Proc. Natl Acad. Sci. USA*, **97**, 6521–6526.
31. Klimov, D. K. & Thirumalai, D. (1999). Stretching single-domain proteins: phase diagram and kinetics of force-induced unfolding. *Proc. Natl Acad. Sci. USA*, **96**, 6166–6170.
32. Klimov, D. K. & Thirumalai, D. (2000). Native topology determines force-induced unfolding pathways in globular proteins. *Proc. Natl Acad. Sci. USA*, **97**, 7254–7259.
33. Mayans, O., Wuerges, J., Canela, S., Gautel, M. & Wilmanns, M. (2001). Structural evidence for a possible role of reversible disulphide bridge formation in the elasticity of the muscle protein titin. *Structure (Camb)*, **9**, 331–340.
34. Gao, M., Wilmanns, M. & Schulten, K. (2002). Steered molecular dynamics studies of titin i1 domain unfolding. *Biophys. J.* **83**, 3435–3445.
35. Best, R. B., Li, B., Steward, A., Daggett, V. & Clarke, J. (2001). Can non-mechanical proteins withstand force? Stretching barnase by atomic force microscopy and molecular dynamics simulation. *Biophys. J.* **81**, 2344–2356.
36. Watanabe, K., Muhle-Goll, C., Kellermayer, M. S., Labeit, S. & Granzier, H. (2002). Different molecular mechanics displayed by titin's constitutively and differentially expressed tandem Ig segments. *J. Struct. Biol.* **137**, 248–258.
37. Williams, P. M., Fowler, S. B., Best, R. B., Toca-Herrera, J. L., Scott, K. A., Steward, A. & Clarke, J. (2003). Hidden complexity in the mechanical properties of titin. *Nature*, **422**, 446–449.
38. Marko, J. F. & Siggia, E. D. (1995). Stretching DNA. *Macromolecules*, **28**, 8759–8770.
39. Oesterhelt, F., Oesterhelt, D., Pfeiffer, M., Engel, A., Gaub, H. E. & Muller, D. J. (2000). Unfolding pathways of individual bacteriorhodopsins. *Science*, **288**, 143–146.
40. Grandbois, M., Beyer, M., Rief, M., Clausen-Schaumann, H. & Gaub, H. E. (1999). How strong is a covalent bond? *Science*, **283**, 1727–1730.
41. Paci, E. & Karplus, M. (1999). Forced unfolding of fibronectin type 3 modules: an analysis by biased molecular dynamics simulations. *J. Mol. Biol.* **288**, 441–459.
42. Gao, M., Craig, D., Vogel, V. & Schulten, K. (2002). Identifying unfolding intermediates of FN-III(10) by steered molecular dynamics. *J. Mol. Biol.* **323**, 939–950.
43. Wood, S. J., Wetzel, R., Martin, J. D. & Hurler, M. R. (1995). Prolines and amyloidogenicity in fragments of the Alzheimer's peptide beta/A4. *Biochemistry*, **34**, 724–730.
44. Williams, A. F. & Barclay, A. N. (1988). The immunoglobulin superfamily—domains for cell surface recognition. *Annu. Rev. Immunol.* **6**, 381–405.
45. Hazes, B. & Dijkstra, B. W. (1988). Model building of disulfide bonds in proteins with known three-dimensional structure. *Protein Eng.* **2**, 119–125.
46. Oberhauser, A. F., Marszalek, P. E., Erickson, H. P. & Fernandez, J. M. (1998). The molecular elasticity of the extracellular matrix protein tenascin. *Nature*, **393**, 181–185.
47. Oberhauser, A. F., Hansma, P. K., Carrion-Vazquez, M. & Fernandez, J. M. (2001). Stepwise unfolding of

- titin under force-clamp atomic force microscopy. *Proc. Natl Acad. Sci. USA*, **98**, 468–472.
48. Fisher, T. E., Marszalek, P. E. & Fernandez, J. M. (2000). Stretching single molecules into novel conformations using the atomic force microscope. *Nature Struct. Biol.* **7**, 719–724.

*Edited by W. Baumeister*

*(Received 3 June 2003; received in revised form 15 September 2003; accepted 16 September 2003)*